# AFRL-SN-HS-TR- 2002-039

## RAMAN EXCITED SPIN COHERENCES FOR TURBULENCE IMAGING

MASSACHUSETTS INSTITUTE OF TECHNOLOGY
Dr. Selim Shahriar
Professor Shaoul Ezekiel
77 Massachusetts Avenue
Cambridge MA 02139

FINAL REPORT: MAY 1998 – APRIL 1999

**APPROVED FOR PUBLIC RELEASE**


**AIR FORCE RESEARCH LABORATORY**
**Sensors Directorate**
**80 Scott Dr**
Hanscom AFB MA 01731-2909

**TECHNICAL REPORT**

**Title: Raman Excited Spin Coherences for Turbulence Imaging**

**PUBLICATION REVIEW**

**This report has been reviewed and is approved for publication:**

**APPROVED:**

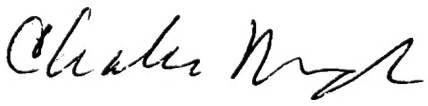

**CHARLES WOODS**
**AFRL/SNHC**
**Optoelectronic Technology Branch**
**Electromagnetics Technology Division**

**APPROVED:**

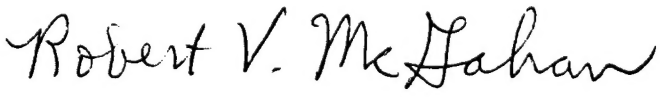

**ROBERT V. McGAHAN**
**Technical Advisor**
**Electromagnetics Technology Division**

# REPORT DOCUMENTATION PAGE

*Form Approved*
*OMB No. 0704-0188*



| 1. AGENCY USE ONLY *(Leave blank)* | 2. REPORT DATE | 3. REPORT TYPE AND DATES COVERED |
|---|---|---|
| | 5 June 2002 | FINAL 1 May 1998 - 30 April 1999 |

**4. TITLE AND SUBTITLE**
Raman Excited Spin Coherences for Turbulence Imaging

**5. FUNDING NUMBERS**
C-F30602-98-2-0016
PE - 61102F
PR - E-8-7216
PROJ - 2305
TA - D7
WU - PF

**6. AUTHOR(S)**
Dr. Selim Shahriar, Prof Shaoul Ezekiel

**7. PERFORMING ORGANIZATION NAME(S) AND ADDRESS(ES)**
Massachusetts Institute of Technolody
77 Massachusetts Avenue
Cambridge, MA 02139

**8. PERFORMING ORGANIZATION REPORT NUMBER**

**9. SPONSORING/MONITORING AGENCY NAME(S) AND ADDRESS(ES)**
Charles Woods
AFRL/SNHC
80 Scott Drive
Hanscom AFB, MA 01731-2909

**10. SPONSORING/MONITORING AGENCY REPORT NUMBER**
AFRL-SN-HS-2002-039

**11. SUPPLEMENTARY NOTES**

**12a. DISTRIBUTION AVAILABILITY STATEMENT**
Approved for public release; distribution unlimited.

**12b. DISTRIBUTION CODE**
a

**13. ABSTRACT** *(Maximum 200 words)*
The objective of this project was to explore the feasibility of using Raman excited spin coherence for turbulence imaging. We experimentally demonstrated that it is possible to use degenerate four-wave mixing (DFWM) in Na vapor to correct intracavity high-speed turbulence aberrations. The use of sodium vapor as a phase conjugate mirror (PCM) provides gains greater than unity and an ideal response time of about 16 nsec, even with cw laser pump beams. We demonstrated a cw degenerate phase conjugate resonator (PCR) using Na vapor with a very low lasing threshold of ~4.5 W/cm2 of pump intensity. This low power threshold is produced by DFWM based on coherent population trapping (CPT) in Na vapor when operating close to the D1 transition. The intracavity turbulence was created by a He jet from a nozzle that was driven at the nozzle's resonance of ~18 kHz. In the intracavity turbulence correction experiment, a typical intensity for the forward and reverse DFWM pump beams is 10W/ cm2. This experiment provided a low-threshold PCR involving a double-$\Lambda$ CPT interaction that produced a correction factor of 9.6 for the temporal aberrations caused by an 18 kHz intracavity turbulence with a flow rate of 250 m/s.

| 14. SUBJECT TERMS | 15. NUMBER OF PAGES |
|---|---|
| phase conjugate mirror | 8 |
| | 16. PRICE CODE |

| 17. SECURITY CLASSIFICATION OF REPORT | 18. SECURITY CLASSIFICATION OF THIS PAGE | 19. SECURITY CLASSIFICATION OF ABSTRACT | 20. LIMITATION OF ABSTRACT |
|---|---|---|---|
| UNCLASSIFIED | UNCLASSIFIED | UNCLASSIFIED | SAR |

Standard Form 298 (Rev. 2-89) (EG)
Prescribed by ANSI Std. 239.18
Designed using Perform Pro, WHS/DIOR, Oct 94

## List of Figures

## Table of Contents

## 1. INTRODUCTION

The objective of this project was to explore the feasibility of using Raman excited spin coherence for turbulence imaging. To this end, we have made substantial progress. The technical achievements in this project are summarized below.

## 2. TECHNICAL ACHIEVEMENT

# Intracavity High-Speed Turbulence Aberration Correction in a Sodium Raman Phase Conjugate Resonator

Optical cavities bounded by a phase conjugate mirror (PCM) with high gain and a conventional mirror are known[1,2] to lase even in the presence of intracavity phase aberrations. Such aberration-compensated phase conjugate resonators (PCR's) have also been utilized for other applications such as associative memories[3], high-resolution optical data processing[4], and imaging threshold detectors[5]. Among several nonlinear optical materials,[1] the use of sodium vapor as the PCM has been shown[2,7] to provide gain greater than unity and an ideal response time of about 16 nsec, even with cw pump lasers. Thus, real-time cw aberration correction at high speed and high gain should be possible in a PCR which uses Na vapor as the PCM. Other PCM materials are known[6] to require high-power pulsed lasers for obtaining fast response time and high gain. A cw PCR using resonant degenerate four-wave mixing (DFWM) in Na vapor was reported, but required very high pump intensities of ~2.5 kW/cm$^2$ and did not demonstrate the ability to operate with intracavity turbulence.[7] In contrast, we demonstrate in this paper a cw degenerate PCR using Na vapor with a very low lasing threshold of ~4.5 W/cm$^2$ of pump intensity. Fast spatio-temporal aberration correction is demonstrated in the presence of a high speed turbulent flow inside the cavity. Such a cw PCR with low pump intensity is made possible by DFWM based on coherent population trapping[8,9] (CPT) in Na vapor when operating close to the $D_1$ transition.

Non-degenerate four-wave mixing (NDFWM)[10] based on CPT involving Raman transitions in Na vapor was shown previously[11] to correct turbulence aberrations in a PCM geometry. A helium jet forced into air at a frequency of 18 kHz and flow velocity of 170 m/s was utilized to demonstrate the spatio-temporal aberration correction. A temporal correction factor of 7.8 was measured at a concurrent power gain of 32 even in the presence of the helium flow. A major difficulty with using such an NDFWM set-up to generate a PCR output at a single frequency is the requirement to match the frequencies of the 'probe' and 'conjugate' beams. Instead of using an electro-optic modulator in the PCR path to match the two frequencies, we demonstrate here high-gain DFWM based on CPT and use it to construct a PCR with an intracavity turbulent jet.

In the PCR experimental arrangement shown in Fig.1, the linearly polarized output of a cw dye laser is split by the beam splitter BS1 into the forward (F) and backward (B) pump beams counterpropagating in the Na vapor cell. The dye laser is

tuned close to the Na $D_1$ transition. The pumps F and B are slightly focused by lenses, L, (f = 1m) to a FWHM diameter of 660 μm at the cell center. An optical isolator, I, prevents feedback into the dye laser from reflections. A PCR cavity is formed between the high-reflectivity (95%) output coupler, R, and the Na cell acting as the high-gain PCM. In the presence of an aberrator in the PCR path, the PCR beam, A, entering the cell would be aberrated, and the PCR beam, C, leaving the cell would be corrected after passing through the aberrator. The conjugate PCR beam, C, is generated primarily by the scattering of B from the grating formed by F and A. The frequencies of the PCR beams A and C generated in this DFWM arrangement is the same as that of F and B. The PCR beam is cross-polarized relative to both F and B. The use of the polarizing beam splitters, PBS, facilitates the steering of A into the cell, and the separation of C from B. The portion of A transmitted through the cell is denoted by 'T' and can exhibit amplification under conditions of gain in the DFWM interaction. The PCR beams A and C are aligned to intercept F and B in the cell at a vertical angle of about 8.5 mrad. The typical FWHM diameters of F and B at the center of the cell are ~0.66 mm, while that of A and C are ~ 0.23mm. The typical optical intensity of F and B at the cell center is about 10 $W/cm^2$ each, unless otherwise stated. The intensity of the PCR beam at the cell center is estimated to be ~ 2.6 $W/cm^2$ at the maximum PCR power of 1.7 mW. The Na vapor cell is a heat-pipe oven operated at ~ 260°C with an ambient pressure of ~ 18 mTorr. No buffer gas is added to the cell. Stray magnetic fields are reduced to less than 20 mG with the use of magnetic shielding around the cell. A telescope, TL, enables mode-matching within the PCR cavity.

A turbulent jet is placed 1m away from a lens, IL, (f = 25cm) which images the jet into the cell with a demagnification of ~67%. This jet is obtained by forcing helium gas at room temperature through a rectangular nozzle (4mm x 0.1mm). The 4mm side of the nozzle is aligned along the PCR path. The nozzle is placed ~ 3mm below the PCR beam path. The nozzle is driven by a PZT transducer at its resonance frequency of 17.8 kHz. The average helium flow speed at the nozzle exit is estimated from the flow rate of 16 cubic foot per hour and the area of the nozzle (0.5 $mm^2$) to be ~ 250m/s.

A CCD camera is utilized to demonstrate spatial aberration correction. The profile of the compensated PCR beam is sampled by the CCD camera at D1 and the aberrated PCR beam profile is sampled at D2. The CCD camera is placed 1.92 m away from the jet when placed at D1, and 0.57m away from the jet at D2. Temporal aberration is measured by directing the PCR output at R (or BS2) onto a 0.3mm pinhole mounted on a photodetector. For the temporal aberration measurements, the PDA replaces the CCD camera at the locations D1 and D2. The transverse location of the PDA is adjusted for maximum amplitude at 17.8 kHz. The ratio of this peak-to-peak ac voltage to the maximum voltage level is termed the modulation depth. This is chosen as the experimental measure of the temporal aberration at the forcing frequency because it compensates for any difference in the intensities of C and A.

Spatial aberration correction is demonstrated in Fig.2 through time-averaged CCD images. The beam profiles are shown both as two-dimensional contour plots at intervals

of 20% of the peak intensity, and as one-dimensional line traces of the intensity at the highest peak location in each profile. The profile of the PCR beam, A, sampled at D2 is shown in Fig.2(a) with the helium flow ON and OFF, while that of the compensated PCR beam, C, sampled at D1 is shown in Fig.2(b) under the same flow conditions. As seen from Figs.2(a) and 2(b), a well-corrected nearly-circular spot is seen at the output coupler R on double-pass through the jet, whereas the uncompensated PCR beam, A, is severely aberrated by the helium jet. The difference in the sizes of the beams C and A shown in Fig.2 is due to the convergence of A as it approaches the imaging lens, IL, from the telescope, TL, and the different distances of D1 and D2 on opposite sides of the jet. The profile of the transmitted PCR beam, T, is sampled at the location D3 which is 0.54 cm away from the cell center (see Fig.1) and is shown in Fig.2(c) with the flow ON and OFF. As expected, the transmitted PCR beam, T, is aberrated by the flow in like manner to A. In the presence of the helium flow, the power in the PCR beams C and A was reduced to half the power with the flow turned off.

Fast temporal aberration correction at 17.8 kHz is demonstrated in Fig.3 through plots of the instantaneous output voltage from the PDA. Here, Fig.3(a) shows the effect of turbulence on the aberrated PCR beam A, while Fig.3(b) shows that for the compensated PCR beam, C. From this data, the signal modulation depth in A is estimated at ~63.6% whereas that in C is ~6.6%, demonstrating that temporal aberrations are corrected by a factor of ~9.6 in the PCR output at R. As discussed in Ref.[11], resonance at higher vibration frequencies result in subharmonics at the output of the PDA and thus are not useful for the measurement of the modulation depth.

In contrast to the NDFWM configuration in Ref.[11], degenerate pumps are used in this DFWM set-up. In order to establish that the system is indeed based on purely DFWM and not NDFWM, the optical frequencies of the PCR beams C and A are determined by mixing with a probe beam, P ( not shown in Fig.1). For this purpose, a small portion of F is tapped off and shifted in frequency by 5 MHz. Such a small shift in optical frequency is achieved by passing the probe beam successively through two acousto-optic modulators (AOM's) driven at 294 and 299 MHz. Figure 4(a) shows the frequency spectrum recorded at the output of an avalanche photodiode (APD) on which the two beams C and P are mixed. Figure 4(b) shows the electrical spectrum of a beat detector mixing the drive frequencies applied as input to the two AOM's. Similar spectra are obtained when A is mixed with P. The 5 MHz separation of the peaks in Figs.4(a) and (b) establishes that DFWM indeed gives rise to C and A. It is also seen from Fig.4(a) that the PCR output spectrum shows only a single peak. Thus, the PCR is oscillating in a single longitudinal mode even without the use of frequency-selective elements within the lasing cavity. For the cavity length of 2.1 m used here, the expected[2] PCR longitudinal mode spacing (c/4L ) is ~36 MHz. Multiple longitudinal modes are not supported in our PCR for the reason that the two-photon bandwidth of the CPT interaction is far lesser, as discussed later.

Figure 5(a) shows the optical power in the PCR beam C as a function of the pump laser frequency. The peaks named I, J and K can be selectively enhanced in power at

their respective frequencies by changing the alignment angle between C (A) and the pumps F and B. Aberration correction measurements described in this paper are done with the peak I enhanced as it occurs at the largest angle of ~ 8.5 mrad from the pumps, thus keeping away from the angular range of conical emission[7,12] that occurs when the pumps are tuned close to the peak K. This conical emission has a typical half-angle of ~ 5mrad or less. When the peak K is enhanced, the angular location of the PCR beams is seen to nearly coincide with the lobes in the hexagonal pattern characteristic of such conical emission. The small broadened peaks between J and K are from diffuse conical emission that is primarily orthogonal in polarization to the PCR beams. The peak I is enhanced when the pump laser frequency is red-detuned by ~300 MHz from the F=2 to the F' =1 transition. It should be noted that the Doppler width of Na vapor at 260°C is ~ 1.1 GHz. Therefore, the detuning measured applies only to the zero-velocity group in the vapor.

The threshold pump intensity at which the PCR output becomes unstable in time was determined (with the flow OFF) by attenuating the total pump power obtained from the laser. The laser frequency was kept fixed at the peak I shown in Fig.5(a). The threshold intensity for each pump was found to be 4.5W/cm$^2$.

To test for CPT, a probe beam, P, with variable frequency relative to F was conjugated. The output coupler R was misaligned to stop oscillation in the PCR mode. However, the experimental operating conditions for this 'PCM' mode remained similar to that for the PCR. The conjugate power gain showed peaks at the same frequencies as I, J, and K shown in Fig.5(a). The laser was tuned to the frequency for peak I. As described earlier, the frequency of P was varied by using the set of two AOM's. Figures 5(b) and 5(c) show the conjugate power gain as a function of the difference frequency between F and P, for two different powers of F. In Fig.5(b) a maximum gain of 3.4 for a probe power of 90 μW is seen at zero difference frequency. The FWHM of the gain is ~2 MHz, far less than the 10 MHz excited state decay rate of Na. This subnatural radio-frequency linewidth for the two-photon interaction is taken as direct evidence for Raman CPT. Another test [9] for Raman CPT is the dependence of the FWHM on the generalized Rabi frequency. As shown in Figs.5(b) and 5(c), the power-broadened linewidth of 2 MHz increases to 3.8 MHz when the pump intensity increases from 4.6 W/cm$^2$ to 10 W/cm$^2$. In order to test the double-Λ nature of the CPT-based DFWM interaction,[11] the conjugate and the probe beams are mixed on an APD. When P is shifted by 1MHz from F (and B), C is found shifted by 2 MHz from the probe, and by 1 MHz from F (and B).

In conclusion, a low-threshold PCR based on DFWM involving a double-Λ CPT interaction has been presented, in which temporal aberrations caused by intracavity turbulence at a frequency of 18 kHz and high speed of 250m/s have been corrected by a factor of 9.6.

**Figure Captions:**

Fig.1. Schematic of the experimental arrangement for a degenerate PCR with intracavity turbulence aberration correction.

Fig.2. Data showing spatial aberration correction: 2-D contours (upper plots) and 1-D line traces (lower plots) of the intensity profile of (a) the aberrated PCR beam, A, (b) the compensated PCR beam, C, and (c) the transmitted PCR beam, T. Contour lines are drawn at 80, 60, 40 and 20 % of peak intensity.

Fig.3. Temporal aberration correction: PPD signal showing turbulence effects on (a) aberrated PCR beam, A, and (b) the compensated PCR beam, C.

Fig.4. Verification of DFWM: (a) the optical beat between C (or A) and the probe P ( shifted by 5 MHz from F), and (b) the electrical voltage spectrum of the two AOM drive signals at 294 and 299 MHz used to generate P.

Fig.5. (a) PCR intracavity power as a function of the pump frequency. The numbers 1 through 4 correspond to the following $D_1$ transitions: (1) $F=2 \leftrightarrow F'=1$ (2) $F=2 \leftrightarrow F'=2$ (3) $F=1 \leftrightarrow F'=1$, and (4) $F=1 \leftrightarrow F'=2$. (b) The PCM conjugate gain as a function of $\Delta f$ for the two pump intensities (i) 4.6 W/cm$^2$ and (ii) 10 W/cm$^2$.

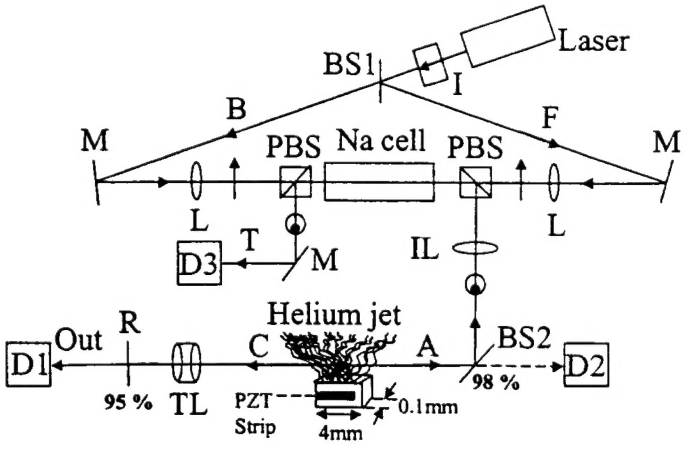

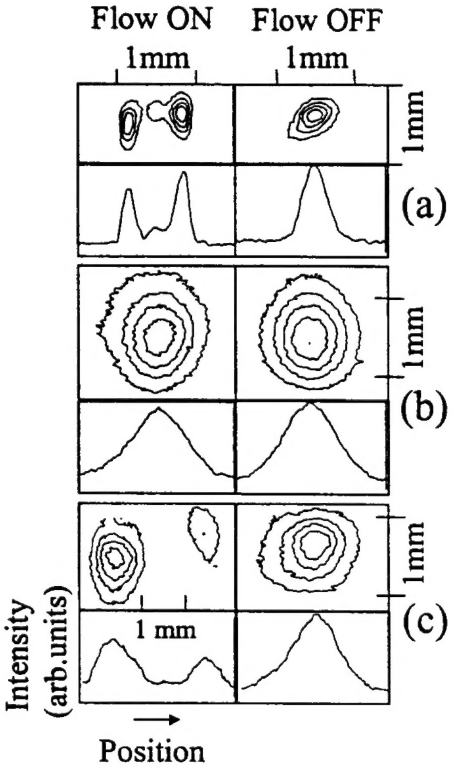
Flow ON
Flow OFF
1mm
1mm
1mm
(a)
1mm
(b)
1mm
(c)
1 mm
Intensity
(arb.units)
Position

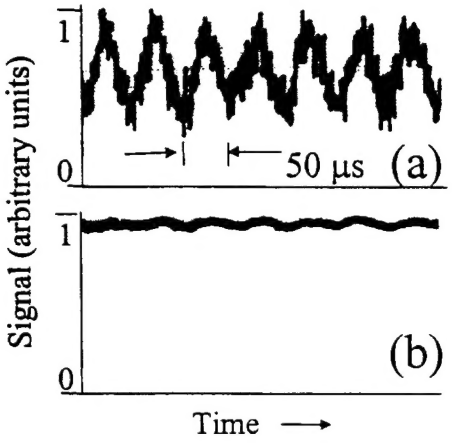
Signal (arbitrary units)
1
0
50 μs
(a)
1
0
(b)
Time

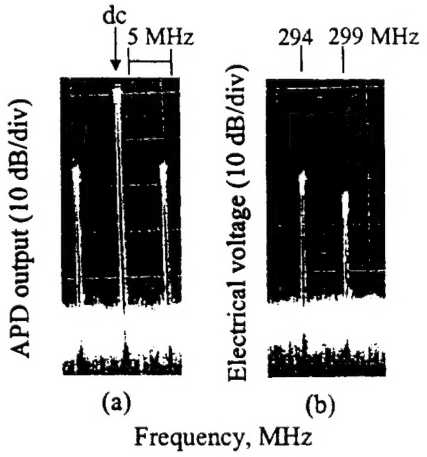
dc
5 MHz
294
299 MHz
APD output (10 dB/div)
Electrical voltage (10 dB/div)
(a)
(b)
Frequency, MHz

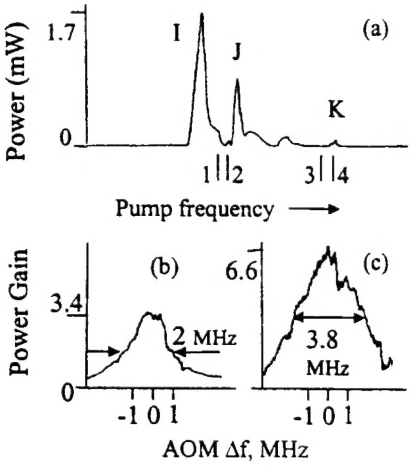


**References**:

1. See, for example, R. A. Fisher, ed., *Optical Phase Conjugation* (Academic, New York, 1983), chapters 13 and 14.
2. R. C. Lind and D. G. Steel, Opt. Lett. **6**, 554 (1981).
3. A. Yariv and S. -K. Kwong, Opt. Lett. **11**, 186 (1986).
4. G. J. Dunning, S. W. McCahon, M. B. Klein, and D. M. Pepper, J. Opt. Soc. Am. **B 11**, 339 (1994).
5. M. B. Klein, G. J. Dunning, G. C. Valley, R. C. Lind, and T. R. O'Meara, Opt. Lett. **11**, 575 (1986).
6. J. R. R. Leite, P. Simoneau, D. Bloch, S. Le Boiteux and M. Ducloy, Europhys. Lett. **2**, 747 (1986).
7. See, for example, B. Monson, G. J. Salamo, A. G. Mott, M. J. Miller, E. J. Sharp, W. W. Clark III, G. L. Wood, and R. R. Neurgaonkar, Opt. Lett. **15**, 12 (1990).
8. H. R. Gray, R. M. Whitley, and C. R. Stroud, Opt. Lett. **3**, 218 (1978).
9. E. Arimondo, in *Progress in Optics XXXV*, E. Wolf, ed. (Elsevier, New York, 1996), pp.258- 354.
10. P. R. Hemmer, D. P. Katz, J. Donoghue, M. Cronin-Golomb, M. S. Shahriar and P. Kumar, Opt. Lett. **20**, 982 (1995).
11. V. S. Sudarshanam, M. Cronin-Golomb, P. R. Hemmer and M. S. Shahriar, Opt.Lett. **22**, 1141 (1997).
12. G. Grynberg, E. Le Bihan, P. Verkerk, P. Simoneau, J. R. R. Leite, D. Bloch, S. Le Boiteux and M. Ducloy, Opt. Commun. **67**, 363, (1988).